PHYSICAL REVIEW B **96**, 140412(R) (2017)

Relieving the frustration through Mn^{3+} substitution in holmium gallium garnet

Paromita Mukherjee,[1,*] Hugh F. J. Glass,[1] Emmanuelle Suard,[2] and Siân E. Dutton[1,*]
[1]*Cavendish Laboratory, University of Cambridge, JJ Thomson Avenue, Cambridge CB3 0HE, United Kingdom*
[2]*Institut Laue-Langevin, 71 Avenue des Martyrs, 38000 Grenoble, France*

(Received 26 April 2017; revised manuscript received 11 September 2017; published 25 October 2017)

We present a Rapid Communication on the impact of Mn^{3+} substitution in the geometrically frustrated Ising garnet $Ho_3Ga_5O_{12}$ using bulk magnetic measurements and low-temperature powder neutron diffraction. We find that the transition temperature $T_N = 5.8$ K for $Ho_3MnGa_4O_{12}$ is raised by a factor of almost 20 when compared to $Ho_3Ga_5O_{12}$. Powder neutron diffraction on $Ho_3Mn_xGa_{5-x}O_{12}$ ($x = 0.5, 1$) below T_N shows the formation of a long-range-ordered state with $\mathbf{k} = (0,0,0)$. Ho^{3+} spins are aligned antiferromagnetically along the six crystallographic axes with no resultant moment, whereas the Mn^{3+} spins are oriented along the body diagonals such that there is a net moment along [111]. The magnetic structure can be visualized as ten-membered rings of corner-sharing triangles of Ho^{3+} spins with the Mn^{3+} spins ferromagnetically coupled to each individual Ho^{3+} spin in the triangle. Substitution of Mn^{3+} completely relieves the magnetic frustration with $f = \theta_{CW}/T_N \sim 1.1$ for $Ho_3MnGa_4O_{12}$.

DOI: 10.1103/PhysRevB.96.140412

In geometrically frustrated magnets the lattice geometry prevents all the magnetic interactions from being satisfied simultaneously. Two consequences of this are a large degeneracy in the number of possible ground states and a suppression of the long-range magnetic ordering temperature. Experimentally it has been observed that factors including symmetric and antisymmetric exchanges, dipolar interactions, crystal electric-field (CEF) effects, and lattice distortions play a role in determining the magnetic properties. Depending on the relative magnitude of competing interactions, the system may be driven into a long-range-ordered state, thus relieving the frustration, or exist in a disordered but correlated state, such as a spin liquid, spin ice, or one with emergent magnetic order [1–8]. Magnetic frustration can also be relieved through site dilution or site disorder of spins [9–13].

Lanthanide garnets with the general formula $Ln_3A_2X_3O_{12}$ are a system containing a highly frustrated magnetic Ln^{3+} lattice. They crystallize in a cubic structure, Fig. 1(a), containing three crystallographic sites for the cations: dodecahedral occupied by Ln, octahedral occupied by A, and tetrahedral occupied by X. The magnetic Ln^{3+} ions lie at the vertices of corner-sharing triangles which form two interpenetrating networks of bifurcated ten-membered rings, Fig. 1(b). The magnetic properties of the lanthanide garnets are highly dependent on the single-ion anisotropy of the Ln^{3+} ion and the cations on the octahedral and tetrahedral sites [14–18]. Much of the experimental and theoretical work so far has focused on the spin liquid candidate gadolinium gallium garnet $Gd_3Ga_5O_{12}$ [15,19–22]. Here we focus on the isostructural holmium gallium garnet $Ho_3Ga_5O_{12}$ (HoGG), which exhibits substantial single-ion anisotropy [23]. $Ho_3Ga_5O_{12}$ was reported to undergo long-range magnetic ordering below 0.19 K in a six sublattice antiferromagnetic structure; however a later neutron-scattering study points to coexistence of long- and short-range magnetic orders below 0.3 K down to 0.05 K [24–26]. We explore the impact of magnetic Mn^{3+} substitution on the magnetic properties and magnetic structure of holmium gallium garnet.

We show that the magnetic frustration of the Ising garnet $Ho_3Ga_5O_{12}$ is relieved almost entirely by partial substitution of nonmagnetic Ga^{3+} with magnetic Mn^{3+}. In the case of $Ho_3Mn_xGa_{5-x}O_{12}$ ($x = 0.5, 1$), the Mn^{3+} spins create a local dipolar field, coupling ferromagnetically with *quasispins* from Ho_3 triangles. The Mn^{3+} spins and the Ho_3 *quasispin* sublattices in $Ho_3MnGa_4O_{12}$ form a long-range-ordered state at $T_N = 5.8$ K, a dramatic contrast to the reported coexistence of short- and long-range orders observed below 0.3 K for unsubstituted $Ho_3Ga_5O_{12}$ [26].

Polycrystalline samples of phase pure $Ho_3Mn_xGa_{5-x}O_{12}$ ($0 \leqslant x \leqslant 1$) have been prepared and the structure evaluated using x-ray and neutron diffraction as described in the Supplemental Material [27]. Mn^{3+} substitution results in a small increase in the unit cell, however no significant changes in the Ho-O bond lengths are observed (see Tables S1 and S2 in the Supplemental Material [27]). Analysis of the crystal structure shows that Mn^{3+} exclusively occupies the octahedral A sites, located above and below each Ho_3 triangle [Fig. 1(c)]. The preference of d^4 Mn^{3+} to occupy only the octahedral sites is expected from consideration of the CEF for the octahedral A and tetrahedral X sites. No evidence for ordering of the Mn^{3+} ions or a Jahn-Teller distortion is observed, although local Jahn-Teller distortions cannot be discounted. At the maximum substitution, 50% of the A sites are occupied by magnetic Mn^{3+} ions. The connectivity of the A sites has been described by one-dimensional chains propagating along the body diagonal of the cubic unit cell [28], however all the sites occupied by Mn^{3+} spins, including those in neighboring chains, are equidistant from one another in the unit cell.

The zero-field-cooled (ZFC) magnetic susceptibility $\chi(T)$ of $Ho_3Mn_xGa_{5-x}O_{12}$ ($0 \leqslant x \leqslant 1$), Fig. 2(a), shows a sharp magnetic ordering transition T_N at 3.5 and 5.8 K for $Ho_3Mn_{0.5}Ga_{4.5}O_{12}$ and $Ho_3MnGa_4O_{12}$, respectively. No ordering is observed in $Ho_3Ga_5O_{12}$ above the limiting temperature of 1.8 K, consistent with previous literature reports [26,29]. The inverse susceptibility χ^{-1} is linear at high temperatures $T > 100$ K [Fig. 2(a) inset], and fits to the

*Corresponding authors: pm545@cam.ac.uk; sed33@cam.ac.uk

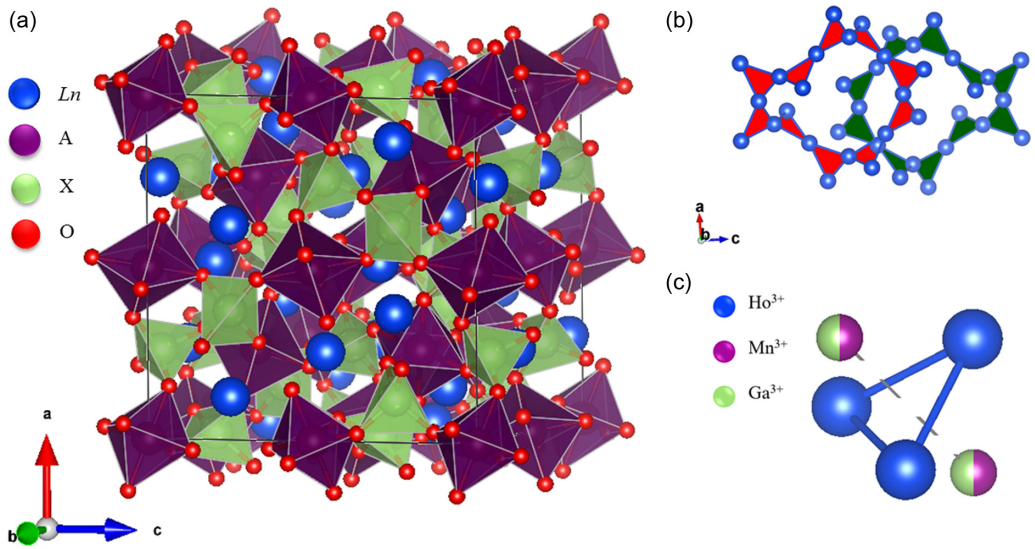

FIG. 1. (a) General crystal structure of lanthanide garnets $Ln_3A_2X_3O_{12}$ with the three cations occupying distinct crystallographic sites—here Ln = Ho, A = Mn/Ga, and X = Ga. (b) Connectivity of magnetic Ho^{3+} ions. The Ho^{3+} ions lie at the vertices of corner-sharing equilateral triangles forming two interpenetrating ten-membered rings. This results in a highly frustrated three-dimensional network. (c) Relative position of Mn^{3+} relative to Ho^{3+}—each triangle with Ho^{3+} at the vertices has a Mn^{3+} atom above and below the centroid of the triangle. Each octahedral site is occupied by Mn^{3+} 25% and 50% of the time for $Ho_3Mn_{0.5}Ga_{4.5}O_{12}$ and $Ho_3MnGa_4O_{12}$, respectively.

Curie-Weiss (CW) law were carried out in different temperature ranges from 100 to 300 K. The difficulty in determining the Weiss temperature θ_{CW} from high-temperature fits to the Curie-Weiss law is well documented for Ho^{3+} containing samples due to the presence of low-lying CEF states [23,26,30]. However, for all compositions, θ_{CW} is negative, indicating net antiferromagnetic interactions. The value of θ_{CW} decreases with an increase in x, indicating weaker antiferromagnetic correlations on Mn^{3+} substitution. The effective moment μ_{eff}, obtained from the Curie-Weiss law (see Table S3 in the Supplemental Material [27]), is underestimated compared to the theoretical moment: $\mu_{th}^2 = 3\mu_{Ho}^2 + x\mu_{Mn}^2$ (this assumes no quenching of the orbital contribution to the effective moment but, partial quenching of the moment would be expected due to presence of low-lying CEF states). However, μ_{eff} increases with x as expected for Mn^{3+} substitution.

Isothermal magnetization curves [Fig. 2(b)] show that the magnetization at 2 K and 9 T, $M_{2\,K,9\,T}$, is significantly increased on Mn^{3+} substitution. The size of the increase cannot solely be attributed to the Mn^{3+} ions as it exceeds the maximum contribution from Mn^{3+} [$M_{Mnmax} = g_S S = 4\,\mu_B$ per formula unit (f.u.)]. The additional increase in magnetization could be due to changes in the underlying magnetism or in the CEF states of Ho^{3+} on substitution. For all samples the observed magnetization at 9 T, $M_{2\,K,9\,T}$, is much lower than the saturation magnetization of a Heisenberg system, $M_{sat} = 3 \times 10 + x \times 4\,\mu_B$/f.u. ($3g_J J + xg_S S$ where $g_J = 5/4, J = 8$ for Ho^{3+} and $g_S = 2, S = 2$ for Mn^{3+}). However, it is consistent with the value expected for powder-averaged Ising Ho^{3+} spins; $M_{sat,Ising} = 3 \times 10/2 + x \times 4\,\mu_B$/f.u. The isothermal magnetization in $Ho_3Ga_5O_{12}$ has previously been shown to be typical of Ising spins [23], and our data are consistent with the Ho^{3+} spins remaining Ising-like on Mn^{3+} substitution. Given their small contribution to the total magnetization, no conclusions can be drawn regarding the isotropy of the Mn^{3+} spins. At 2 K, a field-induced transition is observed at 0.27(1) and 0.46(1) T for $Ho_3Mn_{0.5}Ga_{4.5}O_{12}$ and $Ho_3MnGa_4O_{12}$, respectively (see Fig. S3 in the Supplemental Material [27]). Similar transitions in Ising garnets containing magnetic ions exclusively on the A site have recently been reported [28]. The plot of dM/dH for $Ho_3Ga_5O_{12}$ also shows a feature at low fields of < 0.2 T (see Fig. S3 in the Supplemental Material [27]), however further measurements are required to understand the nature of these field-induced transitions.

To explore the nature of the magnetic ordering, we carried out low-temperature powder neutron-diffraction experiments on $Ho_3Mn_{0.5}Ga_{4.5}O_{12}$ and $Ho_3MnGa_4O_{12}$. Both samples show strong magnetic Bragg peaks below T_N. No magnetic diffuse scattering is observed for either sample at $T \geqslant 1.5$ K, suggesting that unlike in HoGG [26], long- and short-range magnetic orders do not coexist. For both samples, the magnetic Bragg reflections are indexed with the propagation vector $\mathbf{k} = (0,0,0)$. All combinations of irreducible representations for Ho^{3+} and Mn^{3+} ions were tested, however only a model with both ions having the Γ_3^1 irreducible representation (see Table S4 in the Supplemental Material [27]) allowed for a good fit to the data [Fig. 3(a)]. For both samples, the magnitude of the Ho^{3+} and Mn^{3+} moments increases on cooling, although the moments are smaller than the theoretical moment [$g_J\sqrt{J(J+1)} = 10.61\mu_B$ for Ho^{3+} and $g_S\sqrt{S(S+1)} = 4.89\mu_B$ for Mn^{3+} respectively] (see Fig. S4 in the Supplemental Material [27]). This may be due to low-lying CEF effects or screening of the moment. Previous studies of $Ho_3Ga_5O_{12}$ and $Ho_3Al_5O_{12}$ also have reported reduced moments, in close agreement with our results [29,31]. Reduced magnetic moments for Mn^{3+} determined from neutron diffraction also have previously been observed [32].

The magnetic structure, Fig. 3(b), has the same long-range-ordered arrangement of the Ho^{3+} spins as that reported for $Ho_3Ga_5O_{12}$ and $Ho_3Al_5O_{12}$ [25,31]. The 24 Ho^{3+} spins in each unit cell are arranged into six sublattices with the Ho^{3+} spins

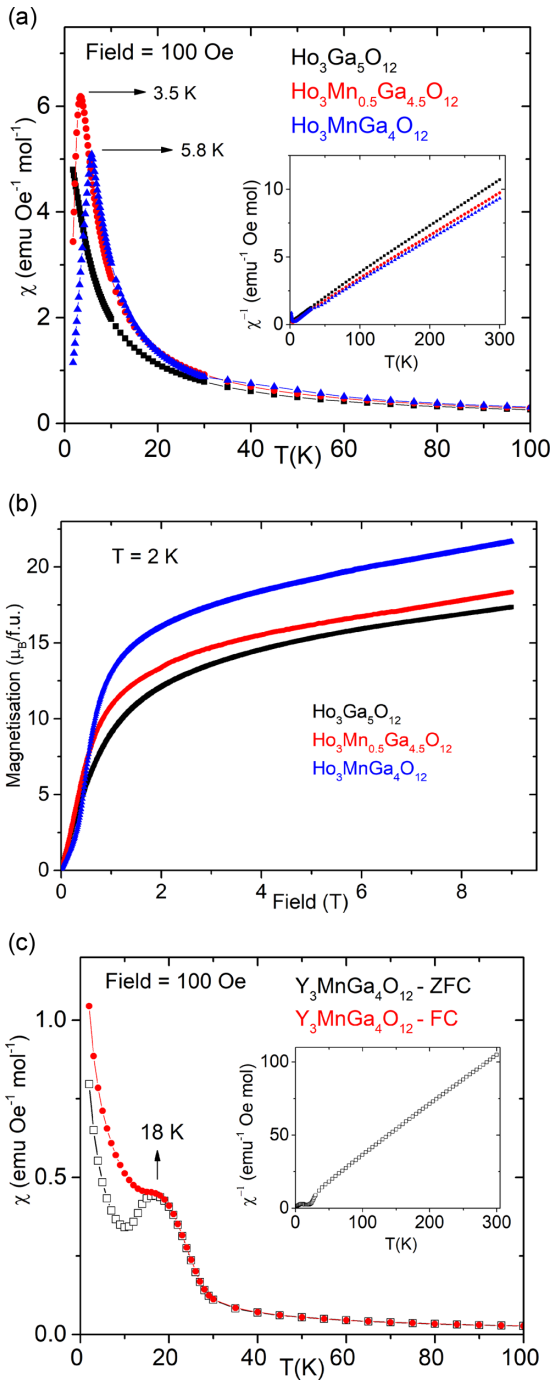

FIG. 2. (a) ZFC magnetic susceptibility $\chi(T)$ measured in 100 Oe for $Ho_3Mn_xGa_{5-x}O_{12}$ ($0 \leqslant x \leqslant 1$): Magnetic ordering transitions are seen clearly at 3.5 and 5.8 K for $x = 0.5$ and $x = 1$, respectively. The inverse magnetic susceptibility χ^{-1} can be seen in the inset. (b) Isothermal magnetization curves at 2 K for $Ho_3Mn_xGa_{5-x}O_{12}$ ($0 \leqslant x \leqslant 1$). (c) ZFC and field-cooled (FC) magnetic susceptibility $\chi(T)$ measured in 100 Oe for $Y_3MnGa_4O_{12}$: A broad spin-glass-like transition is observed at $T_0 = 18$ K. The inverse magnetic susceptibility $\chi^{-1}(T)$ can be seen in the inset.

aligned along the crystallographic axes [100], [$\bar{1}$00], [010], [0$\bar{1}$0], [001], and [00$\bar{1}$] such that the net moment is zero. The Mn^{3+} spins in each unit cell are aligned along the body diagonals as reported for the Ising garnet $CaY_2Co_2Ge_3O_{12}$ [28], however, their relative orientations are completely different. The Mn^{3+} moments are oriented along [111], [$\bar{1}\bar{1}$1], [$\bar{1}$1$\bar{1}$], and [1$\bar{1}\bar{1}$] such that there is a resultant moment from the Mn^{3+} spins along [111]. The relative orientations of the Ho^{3+} and Mn^{3+} spins assume greater significance when we consider the two interpenetrating networks of the ten-membered triangles of the Ho^{3+} spins, Fig. 3(c). For each ten-membered ring, the net magnetic moment of the Ho^{3+} spins is zero, however, there is a net ferromagnetic interaction between the Ho^{3+} and the Mn^{3+} moments. When these interactions are summed over a Ho_3 triangle, then the resultant Ho^{3+} *quasispin* is orientated in or out of the centroid of the triangle, i.e., along [111] [Fig. 3(d)] and are located directly above or below the site partially occupied by Mn^{3+}. The Mn^{3+} spin aligns co-parallel with the Ho_3 *quasispin* [Fig. 3(e)]. Although the construct of the Ho_3 *quasispins* allows for the magnetic structure to be rationalized, it should be noted that, in the parent material $Ho_3Ga_5O_{12}$, coupling between any two of the Ho^{3+} spins on an individual triangle $\propto \boldsymbol{S}_1 \cdot \boldsymbol{S}_2$ results in no net interaction as they are orthogonal, however, in the case of $Ho_3Mn_xGa_{5-x}O_{12}$ each individual Ho^{3+}-Mn^{3+} interaction is nonzero.

To our knowledge the concurrent magnetic ordering observed for both Ho^{3+} and Mn^{3+} in $Ho_3MnGa_4O_{12}$ is unique when compared to other rare-earth–transition-metal oxides with complex magnetic structures. Studies on magnetic dopants in lanthanide garnets have been restricted to $Ln_3Fe_5O_{12}$ where Fe^{3+} occupies both octahedral and tetrahedral sites. The two Fe^{3+} sublattices order in a ferrimagnetic structure at ∼130−140 K whereas the Ln^{3+} ions order in an umbellate structure around ∼10 K [33–35]. In $HoMnO_3$, the Mn^{3+} spins order at ∼72 K, whereas the onset of ordering in the Ho^{3+} spins is seen at the spin-rotation transition for the Mn^{3+} spins ∼33 K followed by an increase in the ordered Ho^{3+} moments below 5 K [36–38]. However, in $Ho_3MnGa_4O_{12}$, no features are observed in the magnetic susceptibility or neutron-diffraction data corresponding to the individual ordering of the Mn^{3+} spins at $T > T_N$. The ordering mechanism is also distinct from the "ordered spin-ice" structure reported for Ho_2CrSbO_7 where the frustration is proposed to be relieved through local ferromagnetic correlations between the Cr^{3+} spins as is evidenced by a positive Curie-Weiss constant for isostructural Y_2CrSbO_7 [13,39]. However, in $Ho_3MnGa_4O_{12}$, the Mn-Mn and Ho-Ho exchange interactions are antiferromagnetic, suggesting that the ordering is driven by a different mechanism, the origin of which is discussed below.

The partial substitution of Ga^{3+} for Mn^{3+} in $Ho_3Mn_xGa_{5-x}O_{12}$ significantly changes the magnetic interactions which need to be considered. In addition to Ho-Ho interactions present in $Ho_3Ga_5O_{12}$, Mn-Mn and Ho-Mn interactions also need to be considered. First we consider the dipolar and exchange interactions between the magnetic Ho^{3+} spins. As the Ho-Ho bond lengths are not changed significantly on Mn^{3+} substitution (see Table S2 in the Supplemental Material [27]), it can be assumed that there is no significant change in the Ho-Ho dipolar interaction energy, $\boldsymbol{D} \sim \frac{\mu_0 \mu_{\text{eff}}^2}{4\pi \boldsymbol{R}_{nn}^3} \sim 0.9$ K. *A priori* calculation of the Ho-Ho exchange interactions is complex as the Curie-Weiss constants for the Mn^{3+} substituted garnets contain contributions from multiple interactions. An order of magnitude approximation for the nearest-neighbor exchange energy J_1 in unsubstituted

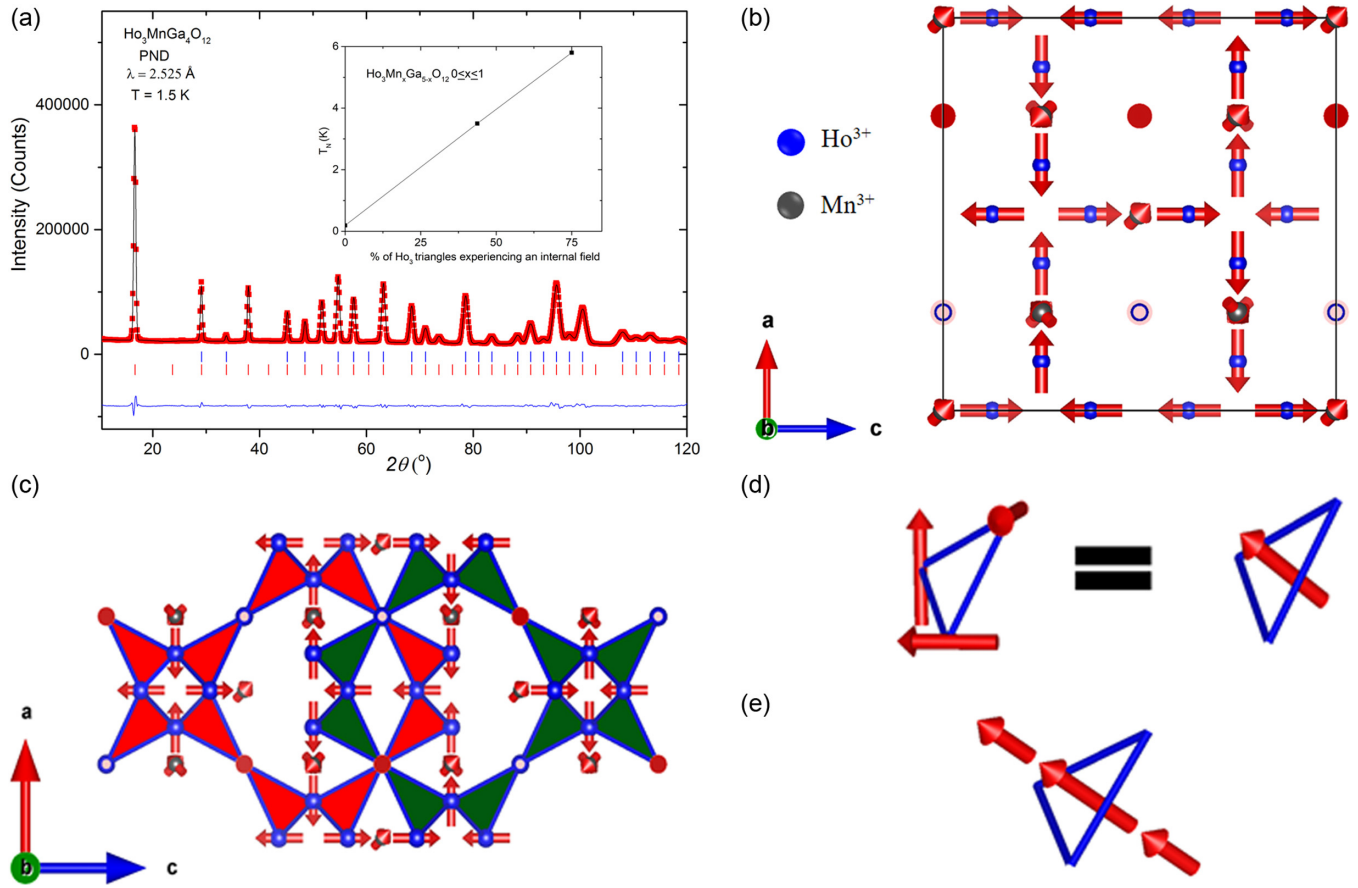

FIG. 3. (a) Rietveld refinement of the neutron-diffraction pattern at 1.5 K for $Ho_3MnGa_4O_{12}$: Blue ticks: nuclear Bragg reflections; red ticks: magnetic Bragg reflections; the inset shows the ordering temperature T_N as a function of the percentage of Ho_3 triangles experiencing the local internal field from the Mn^{3+} spins. (b) Magnetic structure for $Ho_3MnGa_4O_{12}$ ($T_N = 5.8$ K). (c) Arrangement of Ho^{3+} and Mn^{3+} spins for $Ho_3MnGa_4O_{12}$ in the two interpenetrating ten-membered rings in the garnet lattice. (d) Each Ho_3 triangle has three orthogonal spins orientated along the three crystallographic axes, and the Ho^{3+} *quasispin* directed along [111] is shown. (e) The Ho^{3+} *quasispin* couples ferromagnetically with the Mn^{3+} spins located above and below the triangle.

$Ho_3Ga_5O_{12}$ can be obtained as $\boldsymbol{J}_1 \sim \frac{3k_B\theta_{CW}}{2n}$ where n = the number of nearest-neighbor $Ho^{3+} = 4$. This gives $J_1 = -4.5$ K and an order of magnitude estimation of J_1 for $Ho_3Mn_xGa_{5-x}O_{12}$. The Mn-Mn exchange interactions can be approximated by considering isostructural $Y_3MnGa_4O_{12}$ (with an analogous lattice parameter and bond lengths as $Ho_3MnGa_4O_{12}$, see Tables S1 and S2 in the Supplemental Material [27]). Here the only magnetic contribution is from the Mn^{3+} spins. The magnetic susceptibility of $Y_3MnGa_4O_{12}$ is shown in Fig. 2(c). The divergence in the zero-field-cooled and field-cooled data at $T_f = 18$ K is characteristic of spin-glass-like behavior. Given the site disorder, formation of a spin-glass state is not unexpected and has been observed in other systems with dilute spins along [111] [40]. Fits to the Curie-Weiss law between 100 and 300 K give $\mu_{eff} = 4.83\,\mu_B$, consistent with Mn^{3+} spins and $\theta_{CW} = -9(4)$ K, indicating antiferromagnetic interactions between Mn^{3+} spins. This corresponds to $J_1 \sim -6.8$ K if each Mn^{3+} spin is assumed to have two nearest neighbors. Determination of the Ho-Mn exchange interactions is nontrivial, and further inelastic neutron-scattering experiments are required for quantitative analysis. However, the resultant spin structure, although constrained by CEF effects, has a ferromagnetic component between adjacent Ho^{3+} and Mn^{3+} spins, suggesting the resulting moment is not minimized. Finally we consider the Ho-Mn dipolar interactions. The local internal dipolar fields due to the Mn^{3+} spins above and below the Ho_3 triangles can be approximated as $\boldsymbol{\mu_0 H} \sim \frac{\mu_0\mu_{eff}}{2\pi r^3} = \frac{\mu_0 g_S\sqrt{S(S+1)}\mu_B}{2\pi r^3}$ where $g_S = 2, S = 2$ for Mn^{3+} and r is the distance between the centroid of the Ho_3 triangle and the Mn^{3+} spin = 2.65 Å ~ 0.5 T and this corresponds to an energy of $\sim$3.2 K. We find a direct relationship between T_N and the number of *quasispins* experiencing a local magnetic field [Fig. 3(a) inset] when a random distribution of Mn^{3+} is assumed. This indicates that the local internal dipolar field may play a role in the magnetic ordering. In $Ho_3Ga_5O_{12}$, the formation of a long-range-ordered state is observed on application of a 2-T field along [111] [26], and this can be interpreted as equivalent to 25% of the Ho_3 triangles experiencing a local field. Although the nature of field-induced long-range ordering in $Ho_3Ga_5O_{12}$ is unknown, this highlights the role of an applied field in the magnetic ordering in Ising garnets.

In conclusion we find that, in $Ho_3Mn_{0.5}Ga_{4.5}O_{12}$ and $Ho_3MnGa_4O_{12}$, the Mn^{3+} moments, disordered on the octahedral site, couple ferromagnetically with the Ho_3 *quasispins* and lift the degeneracy associated with magnetic ordering in Ising garnets. The elevation of the ordering

temperature almost completely relieves the magnetic frustration $f = |\theta_{CW}/T_N|$[1] such that $f \sim 1.1$ for $Ho_3MnGa_4O_{12}$ compared to $f \sim 40$ for $Ho_3Ga_5O_{12}$ (see the Supplemental Material [27]). Susceptibility measurements show similar increases in T_N for $Ln_3Mn_xGa_{5-x}O_{12}$ (Ln = Tb,Dy). The Cr^{3+} substituted lanthanide gallium garnets $Ln_3CrGa_4O_{12}$ (Ln = Tb,Dy,Ho) also show an increase in T_N by a smaller factor than on Mn^{3+} substitution [41]. Neutron diffraction is required to elucidate the magnetic structure in these cases, but this hints at a universal mechanism for relieving the magnetic frustration in Ising lanthanide garnets, which is tunable through control of the extent and type of magnetic ion substitution.

We thank J. Hodkinson for his support during the experiments on D1B, ILL. We acknowledge funding support from the Winton Programme for the Physics of Sustainability. Magnetic measurements were carried out using the Advanced Materials Characterisation Suite, funded by EPSRC Strategic Equipment Grant No. EP/M000524/1.

Supporting data can be found in Ref. [42], neutron diffraction data can also be found in Ref. [43].

[1] A. P. Ramirez, Annu. Rev. Mater. Sci. **24**, 453 (1994).
[2] J. E. Greedan, J. Mater. Chem. **11**, 37 (2001).
[3] L. Balents, Nature (London) **464**, 199 (2010).
[4] J. S. Gardner, B. D. Gaulin, A. J. Berlinsky, P. Waldron, S. R. Dunsiger, N. P. Raju, and J. E. Greedan, Phys. Rev. B **64**, 224416 (2001).
[5] K. A. Ross, L. Savary, B. D. Gaulin, and L. Balents, Phys. Rev. X **1**, 021002 (2011).
[6] P. P. Deen, O. A. Petrenko, G. Balakrishnan, B. D. Rainford, C. Ritter, L. Capogna, H. Mutka, and T. Fennell, Phys. Rev. B **82**, 174408 (2010).
[7] S. T. Bramwell, Science **294**, 1495 (2001).
[8] J. A. M. Paddison, H. S. Ong, J. O. Hamp, P. Mukherjee, X. Bai, M. G. Tucker, N. P. Butch, C. Castelnovo, M. Mourigal, and S. E. Dutton, Nat. Commun. **7**, 13842 (2016).
[9] L. Yan, F. Maciá, Z. Jiang, J. Shen, L. He, and F. Wang, J. Phys.: Condens. Matter **20**, 255203 (2008).
[10] B. C. Melot, J. E. Drewes, R. Seshadri, E. M. Stoudenmire, and A. P. Ramirez, J. Phys.: Condens. Matter **21**, 216007 (2009).
[11] H. D. Zhou, J. Lu, R. Vasic, B. W. Vogt, J. A. Janik, J. S. Brooks, and C. R. Wiebe, Phys. Rev. B **75**, 132406 (2007).
[12] M. Morin, E. Canévet, A. Raynaud, M. Bartkowiak, D. Sheptyakov, V. Ban, M. Kenzelmann, E. Pomjakushina, K. Conder, and M. Medarde, Nat. Commun. **7**, 13758 (2016).
[13] M. J. Whitaker and C. Greaves, J. Solid State Chem. **215**, 171 (2014).
[14] C. P. Reshmi, S. Savitha Pillai, K. G. Suresh, and M. R. Varma, J. Magn. Magn. Mater. **324**, 1962 (2012).
[15] J. A. M. Paddison, H. Jacobsen, O. A. Petrenko, M. T. Fernandez-Diaz, P. P. Deen, and A. L. Goodwin, Science **350**, 179 (2015).
[16] F. Maglia, V. Buscaglia, S. Gennari, P. Ghigna, M. Dapiaggi, A. Speghini, and M. Bettinelli, J. Phys. Chem. B **110**, 6561 (2006).
[17] J. A. Quilliam, S. Meng, H. A. Craig, L. R. Corruccini, G. Balakrishnan, O. A. Petrenko, A. Gomez, S. W. Kycia, M. J. P. Gingras, and J. B. Kycia, Phys. Rev. B **87**, 174421 (2013).
[18] P. Mukherjee, A. C. Sackville Hamilton, H. F. J. Glass, and S. E. Dutton, J. Phys.: Condens. Matter **29**, 405808 (2017).
[19] P. Schiffer, A. P. Ramirez, D. A. Huse, P. L. Gammel, U. Yaron, D. J. Bishop, and A. J. Valentino, Phys. Rev. Lett. **74**, 2379 (1995).
[20] A. C. Sackville Hamilton, G. I. Lampronti, S. E. Rowley, and S. E. Dutton, J. Phys.: Condens. Matter **26**, 116001 (2014).
[21] N. d'Ambrumenil, O. A. Petrenko, H. Mutka, and P. P. Deen, Phys. Rev. Lett. **114**, 227203 (2015).
[22] N. Woo, D. M. Silevitch, C. Ferri, S. Ghosh, and T. F. Rosenbaum, J. Phys.: Condens. Matter **27**, 296001 (2015).
[23] B. L. Reid, D. F. McMorrow, P. W. Mitchell, O. Prakash, and A. P. Murani, Phys. B: Condens. Matter **174**, 51 (1991).
[24] J. Hamman and P. Manneville, J. Phys. (France) **34**, 615 (1973).
[25] J. Hammann and M. Ocio, J. Phys. (France) **38**, 463 (1977).
[26] H. D. Zhou, C. R. Wiebe, L. Balicas, Y. J. Yo, Y. Qiu, J. R. D. Copley, and J. S. Gardner, Phys. Rev. B **78**, 140406 (2008).
[27] See Supplemental Material at http://link.aps.org/supplemental/10.1103/PhysRevB.96.140412 for the details of sample preparation, experimental methods, structural Rietveld refinement of x-ray and neutron diffraction patterns, crystallographic parameters including bond lengths, parameters from bulk magnetic measurements, irreducible representation for the magnetic structure and ordered magnetic moment as a function of temperature.
[28] A. J. Neer, J. A. Milam-Guerrero, J. E. So, B. C. Melot, K. A. Ross, Z. Hulvey, C. M. Brown, A. A. Sokol, and D. O. Scanlon, Phys. Rev. B **95**, 144419 (2017).
[29] J. Hammann and M. Ocio, Physica B+C **86–88**, 1153 (1977).
[30] A. L. Cornelius and J. S. Gardner, Phys. Rev. B **64**, 060406(R) (2001).
[31] J. Hammann, Acta Crystallogr. Sect. B **25**, 1853 (1969).
[32] A. Muñoz, J. A. Alonso, M. J. Martínez-Lope, M. T. Casáis, J. L. Martínez, and M. T. Fernández-Díaz, Phys. Rev. B **62**, 9498 (2000).
[33] D. Rodic, M. Mitric, R. Tellgren, H. Rundlof, and A. Kremenovic, J. Magn. Magn. Mater. **191**, 137 (1999).
[34] M. Guillot, A. Marchand, F. Tchéou, and P. Feldmann, J. Appl. Phys. **53**, 2719 (1982).
[35] M. Lahoubi, W. Younsi, M.-L. Soltani, and B. Ouladdiaf, J. Phys.: Conf. Ser. **200**, 82018 (2010).
[36] A. Muñoz, J. A. Alonso, M. J. Martínez-Lope, M. T. Casáis, J. L. Martínez, and M. T. Fernández-Díaz, Chem. Mater. **13**, 1497 (2001).
[37] F. Yen, C. R. Dela Cruz, B. Lorenz, Y. Y. Sun, Y. Q. Wang, M. M. Gospodinov, and C. W. Chu, Phys. Rev. B **71**, 180407 (2005).
[38] O. P. Vajk, M. Kenzelmann, J. W. Lynn, S. B. Kim, and S. W. Cheong, J. Appl. Phys. **99**, 08E301 (2006).
[39] L. Shen, C. Greaves, R. Riyat, T. C. Hansen, and E. Blackburn, Phys. Rev. B **96**, 094438 (2017).
[40] S. E. Dutton, P. D. Battle, F. Grandjean, G. J. Long, and K. Oh-Ishi, Inorg. Chem. **47**, 11212 (2008).
[41] P. Mukherjee and S. E. Dutton, Adv. Funct. Mater. **27**, 1701950 (2017).
[42] https://doi.org/10.17863/CAM.13758.
[43] https://doi.org/10.5291/ILL-DATA.5-31-2457.